Journal of Fluorine Chemistry 178 (2015) 14–22

Contents lists available at ScienceDirect

Journal of Fluorine Chemistry

journal homepage: www.elsevier.com/locate/fluor

Electrochemical study of the corrosion of a Ni-based alloy GH3535 in molten (Li,Na,K)F at 700 °C

Yanli Wang [a], Huijun Liu [a], Guojun Yu [b], Juan Hou [b], Chaoliu Zeng [a,*]

[a] Laboratory for Corrosion and Protection, Institute of Metal Research, Chinese Academy of Sciences, 62 Wencui Road, Shenyang 110016, China
[b] Shanghai Institute of Applied Physics, Chinese Academy of Sciences, 2019 Jialuo Road, Shanghai 201800, China

ARTICLE INFO

Article history:
Received 31 December 2014
Received in revised form 26 April 2015
Accepted 16 June 2015
Available online 23 June 2015

Keywords:
Ni-based alloy GH3535
Molten fluorides
Corrosion
Chromium fluorides
Electrochemical techniques

ABSTRACT

The compatibility of structural materials with molten fluoride salts is an immediate challenge for the application and development of molten salt reactor (MSR) operating at high temperatures. In the present presentation, the corrosion behavior of a nickel-based alloy GH3535 has been examined in an eutectic (Li,Na,K)F melt at 700 °C under Ar and Ar-5%H_2O, respectively, by some electrochemical techniques. Moreover, the effect of the additive CrF_3 with concentrations of 0.09 and 0.18 M on the corrosion of the alloy in the melt has also been investigated in an attempt to understand the corrosion mechanism involving the multivalent transition metal Cr ions Cr^{2+}/Cr^{3+}. It is shown that the alloy is in active dissolution state at the corrosion potential and its corrosion occurs mainly through the preferential dissolution of Cr from the substrate, producing a Cr-depleted layer and some internal voids. The introduction of 5%H_2O in Ar accelerates obviously the corrosion of the alloy, giving rise to the formation of a wider Cr-depleted layer where some Cr-rich internal oxides are formed over the internal voids. CrF_3 itself acts as an oxidizer to accelerate the dissolution of Cr, with a more significant effectiveness observed for a higher CrF_3 content.

1. Introduction

Molten fluoride salts such as LiF-NaF-KF and LiF-BeF_2 appear to be excellent candidates as fuel carrier and coolant in molten salt reactors (MSR) due to their advantages of good thermal conductivity, large specific heat, low viscosity, low vapor pressure at operating temperatures, low melting point, high boiling point and relatively good chemical inertness [1]. However, an immediate challenge for the application of molten fluorides in MSR is the material compatibility with the corrosive molten fluorides at high operating temperatures. Over the past 60 years, great efforts have been devoted to the issues of materials and corrosion with molten fluoride salts. In molten fluorides, most oxide films are chemically unstable, and thus the corrosion occurs mainly through the dissolution of alloying elements into the melts. The impurities in fluoride salts such as H_2O and oxides, temperature gradient and galvanic corrosion have been considered as the main driving forces for the corrosion in molten fluorides [2,3].

As a common impurity, H_2O is extremely hard to be removed completely. It may react with molten fluorides to generate HF which then attacks metals to form metal fluorides. The increase in the content of impurities may make the melts be more aggressive, and thus increase the corrosion rate. In a study of the effect of moisture on the corrosion of Ni-based alloys in molten (Li,Na,K)F, Ouyang et al. observed that higher moisture content would aggravate intergranular corrosion and pitting [4]. Kondo et al. also reported that the corrosion of JLF-1 in the purified (Li,Na,K)F was much less than that in the non-purified (Li,Na,K)F [5]. In addition, multivalent transition metals ions such as Cr^{2+}/Cr^{3+}, Fe^{2+}/Fe^{3+} are expected to be present in MSR due to disproportionation reaction and dissolution. The high-valence ions such as Cr^{3+} may also act as an oxidizer to accelerate the dissolution of Cr.

When a metal is in electrical contact with another metal with more positive electromotive potential in molten fluorides, its dissolution could be accelerated. Moreover, a persistent dissolution may occur in a molten fluoride system with significant temperature gradients.

Because metals with less negative free energies of fluoride formation are less prone to corrosion, more noble metals are suitable for the structural materials of MSR. Ni-based alloys with a low content of Cr have been considered as the most suitable

* Corresponding author. Tel.: +86 24 23904553; fax: +86 24 23893624.
E-mail addresses: liuhj@imr.ac.cn, clzeng@imr.ac.cn (C. Zeng).

http://dx.doi.org/10.1016/j.jfluchem.2015.06.014
0022-1139/

structure materials for MSR, among which Hastelloy-N (Ni–16%Mo–7%Cr–5%Fe, weight percent) developed by ORNL (Oak Ridge National Laboratory, USA) has been successfully used as the container material of an experimental molten salt reactor [6,7].

Up to now, the corrosion in molten fluorides has been investigated mostly by thermogravimetric method [5,8,9] by which, however, the corrosion process cannot be examined in situ. The corrosion in molten fluorides is electrochemical in essence, and thereby can be investigated by electrochemical techniques. These electrochemical techniques have been proved effective in understanding the corrosion mechanism and kinetics, with more information obtained for the corrosion processes. There have been some reports on the electrochemical investigation of corrosion in molten fluorides [10–15], but with the emphasis on the determination of oxidation states, suitable electrode materials and basic electrochemical characteristics of specific elements using cyclic voltammetry [13]. Recently, the present authors [14,15] investigated the corrosion behavior of pure Ni, Fe and Cr in molten (Li,Na,K)F by some electrochemical methods and observed dramatic galvanic corrosion, with the most significant galvanic corrosion effect for the couple Ni/Cr [15].

In the present study, the corrosion behavior of a hot rolled Ni-based alloy GH3535 has been examined in molten LiF-NaF-KF under Ar and Ar-5%H_2O, respectively, by electrochemical polarization and impedance techniques. In addition, the effect of multivalent transition metal Cr ions Cr^{3+} on the corrosion of the alloy has also been investigated, with an attempt to understand the corrosion mechanism.

2. Results and discussion

2.1. Potentiodynamic polarization measurements

Fig. 2 shows the potentiodynamic polarization curves of GH3535 in molten (Li,Na,K)F at 700 °C under Ar and Ar-5%H_2O, respectively. In both atmospheres the alloy is all in active dissolution state at the corrosion potential. The presence of 5%H_2O in Ar promotes significantly both the anodic and cathodic reactions, suggesting that H_2O may make the melt be more aggressive and thus give rise to a higher dissolution rate. The corrosion current density (I_{corr}), and the anodic and the cathodic Tafel slopes (b_a and b_c) have been calculated using Tafel extrapolation method, as listed in Table 2. The corrosion potential of the alloy under Ar-5%H_2O is about −432 mV vs. Ni/NiF_2 close to the value of −430 mV vs. Ni/NiF_2 under Ar. However, I_{corr} in Ar-5%H_2O is 374 μA cm^{-2} more than three times the value of 108 μA cm^{-2} in Ar, indicating that the corrosion of the alloy is accelerated significantly by 5%H_2O. In a study of the electrochemical behavior of pure Ni, Fe and Cr in molten (Li,Na,K)F at 700 °C under Ar [15], the present authors reported that I_{corr} of Ni and Cr is 19.3 and 494 μA cm^{-2}, respectively. I_{corr} for GH3535 is significantly lower than that for pure Cr, but still obviously larger than that for pure Ni. F. Fabre et al. also reported a value of 46 μA cm^{-2} for I_{corr} of pure Ni in molten LiF-NaF at 900 °C [11]. The corrosion potential for pure Ni and Cr has been reported to be −0.077 V and −0.507 V vs. Ni/NiF_2, respectively [14]. The corrosion potential of GH3535 is more negative than that of pure Ni, but more positive than that of pure Cr. The increase of the impurity H_2O could increase the redox potential of the melt and thus make the melt be more corrosive. An investigation by Ignat'ev et al. indicated that the redox potential of NaF-LiF-BeF_2 could be decreased from 1.78 to 1.1 V relative to a beryllium comparison electrode by removing the impurities from the melt [16]. It is clear that the increase in the impurity H_2O could accelerate the corrosion of GH3535, and the corrosion rate of a Cr-containing alloy is related to the Cr content, with a higher rate for a higher Cr content.

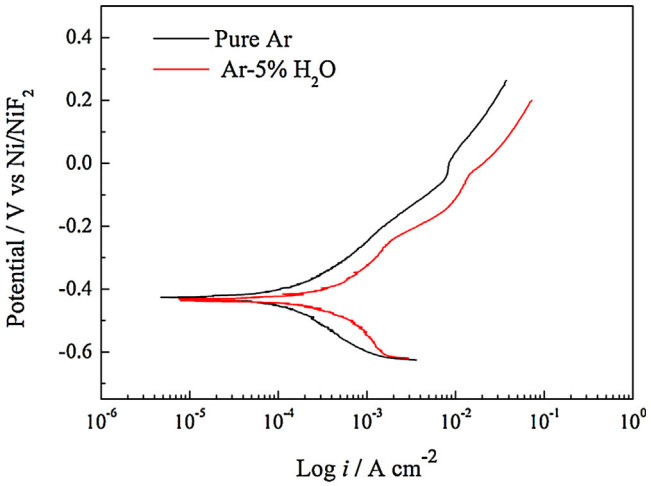

Fig. 2. Potentiodynamic polarization curves of GH3535 at 700 °C in molten (Li,Na,K)F under Ar and Ar-5%H_2O.

Fig. 3 presents the potentiodynamic polarization curves of GH3535 in the melt with and without CrF_3. It is clear that the cathodic reaction is accelerated greatly by CrF_3, with a more obvious effectiveness observed for a higher content of CrF_3. The anodic reaction is also promoted, especially for the melt containing 0.18 M CrF_3. The free corrosion current density of the alloy is calculated to 0.84 mA cm^{-2} for 0.09 M CrF_3 and 2.06 mA cm^{-2} for 0.18 M CrF_3 which are all significantly higher than that for the melt without CrF_3.

2.2. Electrochemical impedance spectra

Fig. 4 gives the typical Nyquist and Bode plots of GH3535 after corrosion in the melt under Ar for various lengths of time. During the experimental duration of 100 h, the Nyquist plots are similar and are all composed of a capacitive loop. The impedance value tends to increase slightly with exposure time.

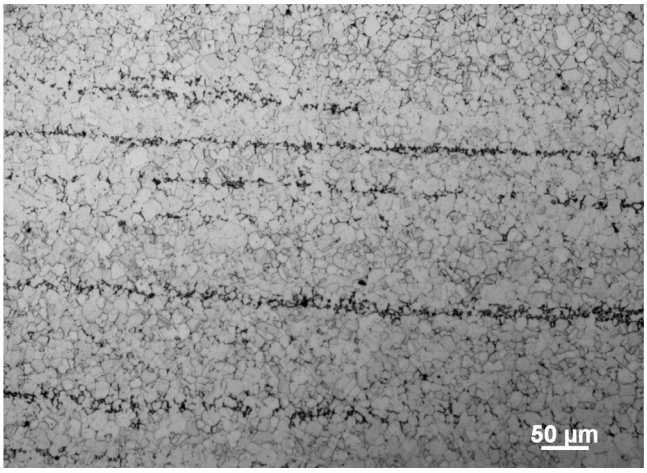

Fig. 1. Microstructure of GH3535 (etched).

Table 1
Chemical composition of the Ni-based alloy GH3535 (in weight percent).

C	Mo	Cr	Fe	Mn	Si	Al	W	Ti	P	S	B	Ni
0.015	17.1	7.03	4.03	0.77	0.59	0.03	0.02	<0.01	0.004	0.001	0.0009	bal.

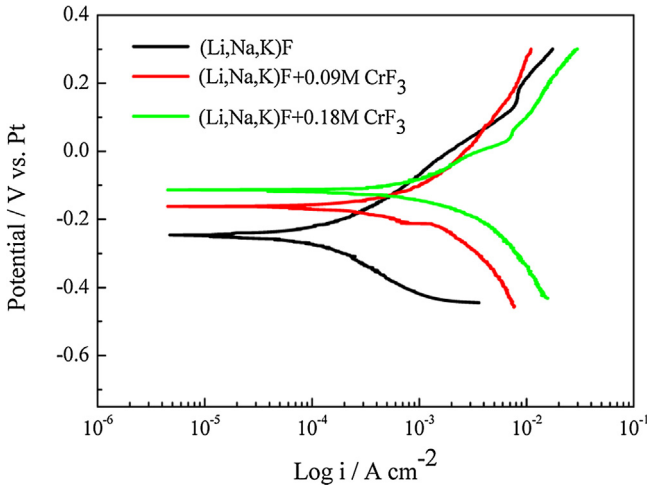

Fig. 3. Potentiodynamic polarization curves of GH3535 at 700 °C under Ar in molten (Li,Na,K)F-CrF_3 containing 0.09 M CrF_3 and 0.18 M CrF_3, respectively.

The impedance plots (Fig. 5) for the corrosion of the alloy in Ar-5%H_2O are similar to those in Ar, but with significantly smaller impedance values, suggesting that the presence of 5%H_2O accelerates greatly the corrosion of GH3535.

Figs. 6 and 7 show the typical Nyquist and Bode plots of GH3535 after corrosion in the melt containing 0.09 M and 0.18 M CrF_3, respectively, under Ar for various lengths of time. The Nyquist plots are all composed of a capacitive loop, with smaller impedance values observed for a higher concentration of CrF_3.

The impedance spectra can be fitted by an equivalent circuit of Fig. 8 where R_s represents the molten salts resistance, C_{dl} the double-layer capacitance and R_t the charge transfer resistance. In the fitting procedure a constant phase angle element (CPE) Q_{dl} is used to replace the element C_{dl}. The impedance of CPE is expressed as

$$Z_{CPE} = \frac{1}{Y_0(jw)^n} \quad (1)$$

Thus, the total impedance of Fig. 8 can be expressed as:

$$Z = R_s + \frac{1}{Y_{dl}(j\omega)^{n_{dl}} + (1/R_t)} \quad (2)$$

where Y_{dl} and n_{dl} are constants representing the element Q_{dl}.

Table 2
Electrochemical parameters obtained from the potentiodynamic polarization curves of GH3535 at 700 °C in molten (Li,Na,K)F under Ar and Ar-5%H_2O, respectively.

	b_a (mV dec^{-1})	b_c (mV dec^{-1})	E_{corr} (mV vs. Ni/NiF_2)	I_{corr} (μA cm^{-2})
Pure Ar	203	176	−432	108
Ar-5%H_2O	265	279	−430	374

Based on the equivalent circuit, the impedance spectra have been fitted and some parameters are listed in Tables 3–6. Figs. 4–7 show clearly that the fitting results are quite good, suggesting that the proposed equivalent circuit is reasonable.

A comparison of Tables 3 and 4 shows clearly that the values of R_t for the corrosion of GH3535 in the melt under Ar are significantly larger than those under Ar + 5%H_2O, indicating a higher corrosion rate in the presence of 5%H_2O. The electrochemical impedance results are in a good accord with the potentiodynamic polarization results.

Tables 5 and 6 indicate that the charge transfer resistance R_t for the corrosion of GH3535 in the melt containing 0.09 M CrF_3 is decreased to the level of 100 Ω cm^2 and to 20 Ω cm^2 in the melt containing 0.18 M CrF_3 which are significantly smaller than those for the melt without CrF_3, suggesting that CrF_3 promotes obviously the corrosion of the alloy in molten (Li,Na,K)F.

The above impedance results demonstrate that the rate-controlling step for the corrosion of GH3535 in the melt is the charge transfer reactions. The obvious deviation of the parameter n_{dl} from 1 suggest the presence of dispersion effect, probably due to a non-uniform electric field caused by the formation of internal voids.

2.3. Characterization of the corroded GH3535

Fig. 9 shows the cross-sectional morphologies and the corresponding EDX line scans of GH3535 corroded in the melt under Ar for 100 h. It is shown that no scales are formed on the alloy surface. The corrosion of the alloy occurs mainly through the preferential dissolution of Cr from the substrate alloy, forming large amounts of internal voids (Fig. 9a) and a Cr-depleted zone with a depth of around 30 μm. The formation of the voids is mainly related to the aggregation of vacancies left by the outward diffusion of Cr. Beneath the internal corrosion zone, some small Mo-rich carbides (bright) precipitate along the grain boundaries (Fig. 9c).

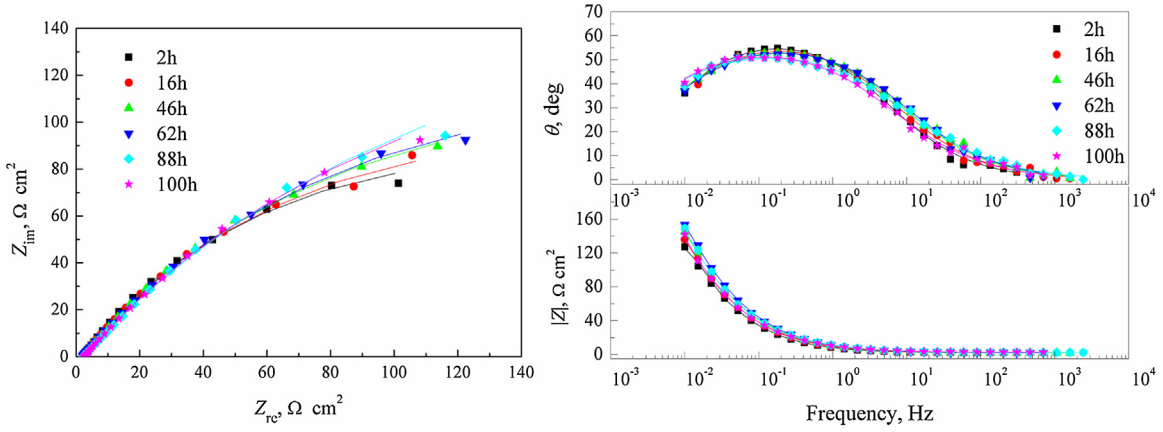

Fig. 4. Nyquist and Bode plots for the corrosion of GH3535 at 700 °C in molten (Li,Na,K)F under Ar for various lengths of time. Symbol: experimental data; line: simulation data.

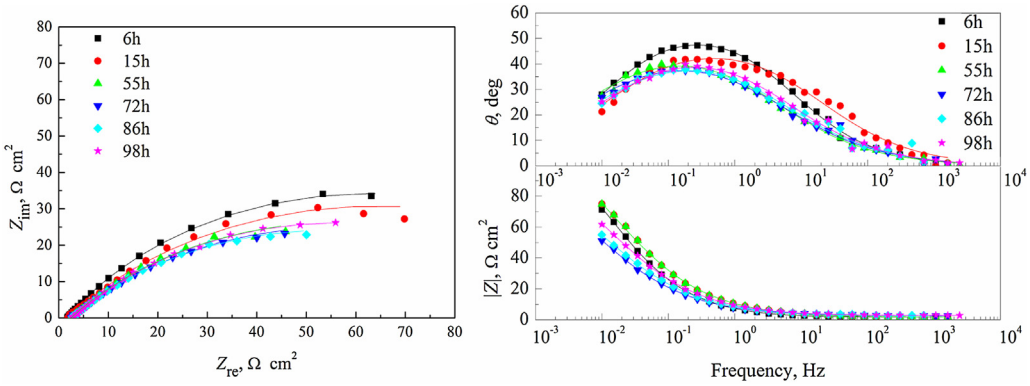

Fig. 5. Nyquist and Bode plots for the corrosion of GH3535 in molten (Li,Na,K)F at 700 °C under Ar-5%H_2O for various lengths of time. Symbol: experimental data; line: simulation data.

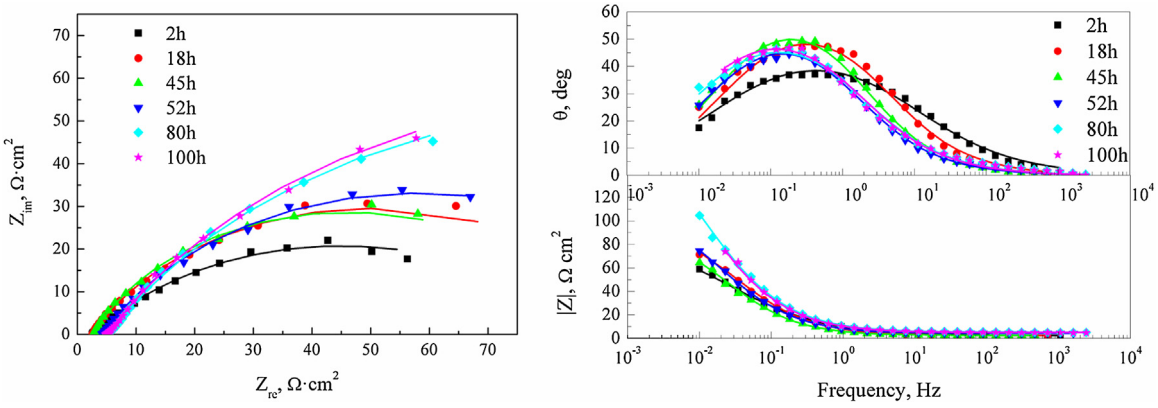

Fig. 6. Nyquist and Bode plots for the corrosion of GH3535 in molten (Li,Na,K)F + 0.09 M CrF_3 at 700 °C under Ar for various lengths of time. Symbol: experimental data; line: simulation data.

Fig. 10 gives the cross-sectional morphologies and the corresponding EDX line scans of the alloy corroded in the melt under Ar-5%H_2O. No scales are formed on the alloy surface, as observed under Ar. However, the alloy is corroded more severely under Ar-5%H_2O than under Ar. In addition to the formation of some internal voids and a Cr-depleted layer with a depth of about 40 μm, some internal Cr-rich oxides are also formed over the internal void layer, with a chemical composition of Ni–30Cr–68O (in atom percent) for the point 2 shown in Fig. 10c. The internal Cr-rich oxides are mainly composed of Cr_2O_3. Ar-5%H_2O atmosphere provides relatively high oxygen and fluorine pressures. During the corrosion, in addition to the outward diffusion of Cr to be dissolved in the melt, fluorine may also diffuse inward to react with Cr in the substrate to form chromium fluorides. Then, the generated Cr fluorides diffuse outward to be oxidized to form internal Cr oxides and release fluorine again at the places with high enough oxygen pressure.

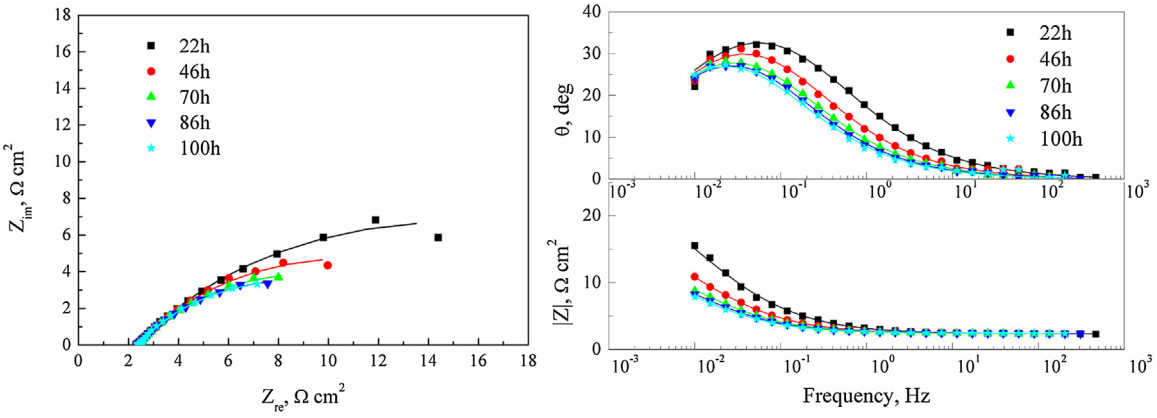

Fig. 7. Nyquist and Bode plots for the corrosion of GH3535 in molten (Li,Na,K)F + 0.18 M CrF_3 at 700 °C under Ar for various lengths of time. Symbol: experimental data; line: simulation data.

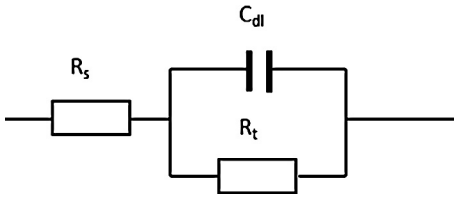

Fig. 8. An equivalent circuit for fitting the impedance spectra.

Fig. 11 gives the cross-sectional morphologies of GH3535 corroded in molten (Li,Na,K)F-CrF_3 for 100 h. It is shown clearly that CrF_3 accelerates greatly the corrosion of the alloy, giving rise to the formation of more internal voids and thicker Cr-depleted layers with a depth of around 80 μm for 0.09 M CrF_3 and 150 μm for 0.18 M CrF_3. It is clear that the presence of substantial concentrations of Cr^{3+} in the melt accelerates greatly the corrosion of the alloy, with a more significant effectiveness observed for a higher CrF_3 content.

2.4. Discussion

The above results indicate that the alloy GH3535 is in active dissolution state at the corrosion potential, and its corrosion goes on mainly through the preferential dissolution of Cr into the melt, giving rise to the formation of many internal voids and a Cr-depleted zone. The presence of 5%H_2O in Ar accelerates obviously the dissolution of Cr, and simultaneously causes the formation of some internal Cr-rich oxides along the substrate. The additive CrF_3 can make the (Li,Na,K)F melt be more aggressive, leading to a higher corrosion rate.

Most oxide films formed on the alloy surface at high temperatures in oxidizing environments are chemically unstable in molten fluorides, as observed in the present study, and thus the corrosion is generally characterized by the thermodynamically driven dissolution of alloying elements into the melt. In the present investigation, the main driving force for the corrosion of GH3535 is the impurity H_2O which is among the most deleterious impurities in molten fluorides from the viewpoint of corrosion and is

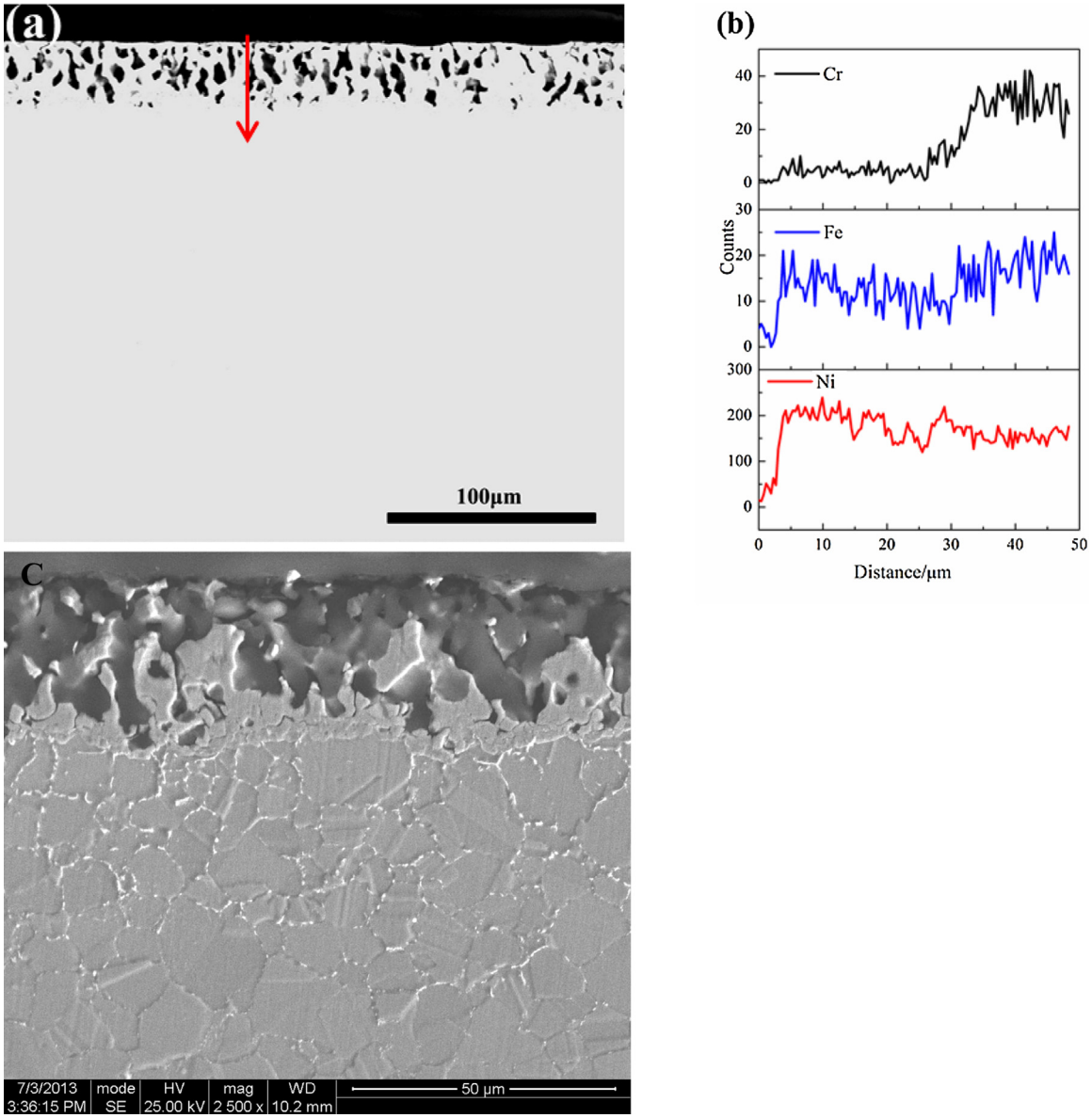

Fig. 9. Cross-sectional morphologies (a and c) and corresponding EDX line scans (b) of GH3535 after corrosion in molten (Li,Na,K)F at 700 °C for 100 h under Ar. (a) un-etched; (c) etched.

Table 3
Fitting results of the impedance spectra for the corrosion of GH3535 in molten (Li,Na,K)F at 700 °C under Ar.

Time (h)	R_s (Ω cm^2)	Y_{dl} (Ω^{-1} cm^{-2} s^{-n})	n_{dl}	R_t (Ω cm^2)
2	2.10	3.89×10^{-2}	0.70	267.8
5	2.06	3.72×10^{-2}	0.69	288.6
8	2.08	3.72×10^{-2}	0.68	300.5
10	2.05	3.69×10^{-2}	0.68	328.9
14	2.02	3.57×10^{-2}	0.68	315.1
16	2.05	3.51×10^{-2}	0.68	300.9
25	2.08	3.42×10^{-2}	0.68	279
38	2.08	3.43×10^{-2}	0.68	359.6
46	2.06	3.24×10^{-2}	0.67	349.0
62	2.11	3.01×10^{-2}	0.67	360.7
72	2.16	3.13×10^{-2}	0.65	373.0
84	2.30	2.89×10^{-2}	0.65	411.0
88	2.29	3.19×10^{-2}	0.63	489.9
96	2.57	3.49×10^{-2}	0.65	467.6
100	2.59	3.53×10^{-2}	0.65	441.7

Table 4
Fitting results of the impedance spectra for the corrosion of GH3535 in molten (Li,Na,K)F at 700 °C under Ar-5%H_2O.

Time (h)	R_s (Ω cm^2)	Y_{dl} (Ω^{-1} cm^{-2} s^{-n})	n_{dl}	R_t (Ω cm^2)
6	1.74	4.80×10^{-2}	0.65	122.6
15	1.79	3.55×10^{-2}	0.58	125.7
27	1.81	5.24×10^{-2}	0.68	131.4
34	2.00	5.46×10^{-2}	0.57	136.1
47	2.32	6.96×10^{-2}	0.56	102.0
55	2.44	6.43×10^{-2}	0.57	110.1
69	2.57	5.99×10^{-2}	0.56	107.5
72	2.61	5.99×10^{-2}	0.55	109.1
80	2.57	5.66×10^{-2}	0.54	104.1
86	2.71	5.28×10^{-2}	0.56	103.3
93	2.71	4.78×10^{-2}	0.57	105.3
98	2.76	4.56×10^{-2}	0.57	108.3

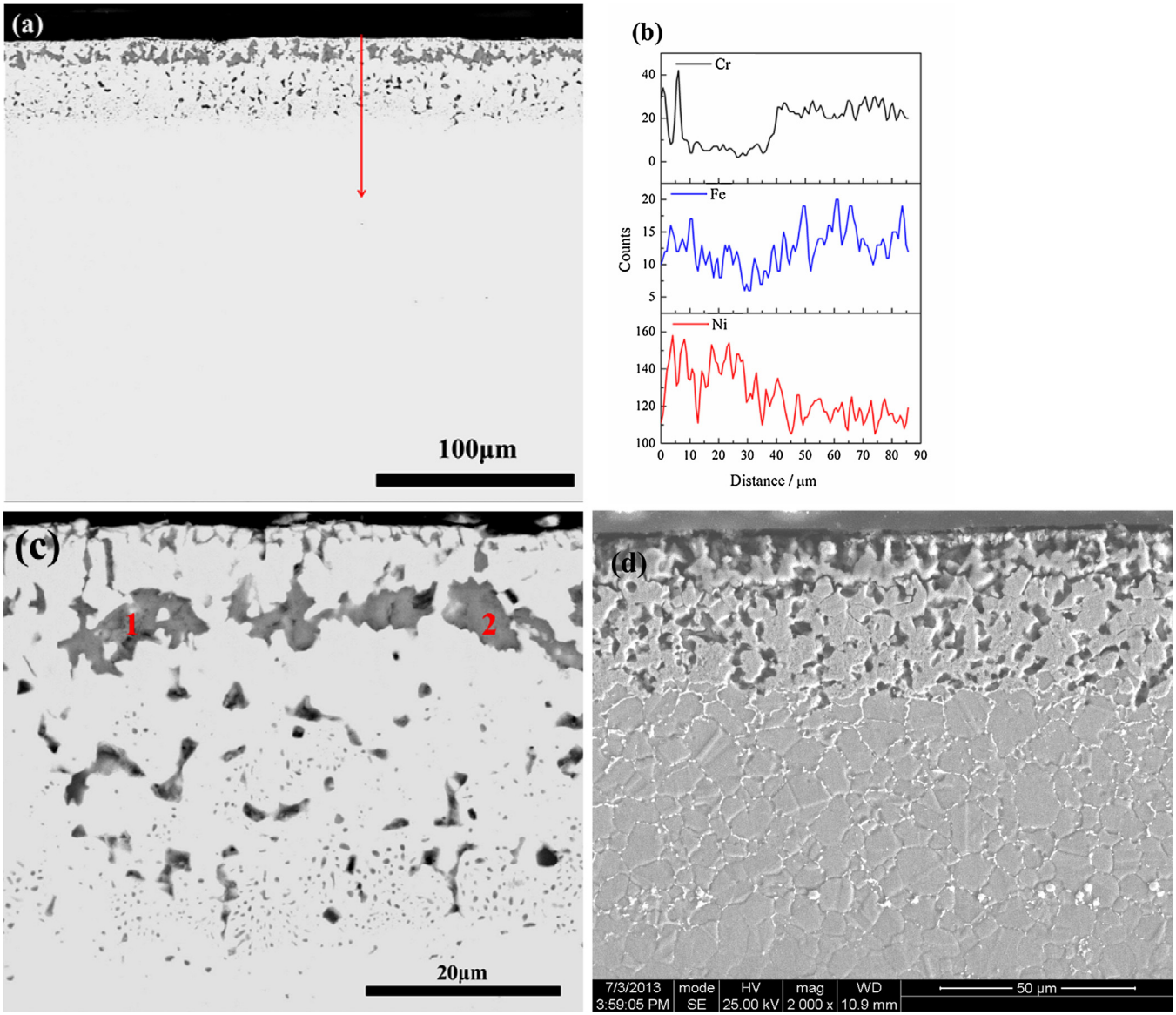

Fig. 10. Cross-sectional morphologies (a, c, and d) and corresponding EDX line scans (b) of GH3535 after corrosion for 100 h in molten (Li,Na,K)F at 700 °C under Ar-5%H_2O. (a) un-etched; (c) amplified view of (a); (d) etched.

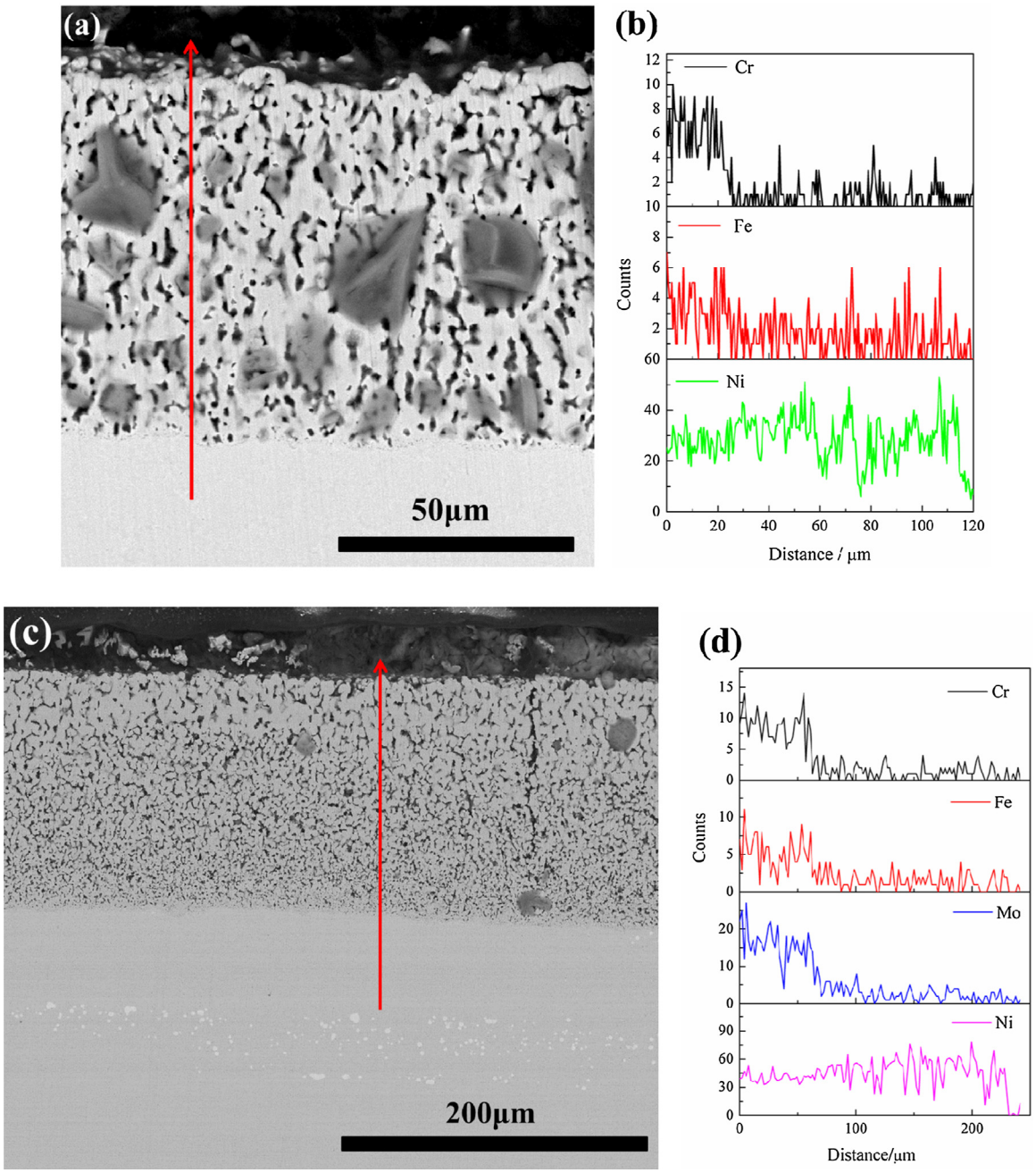

Fig. 11. Cross-sectional morphologies and corresponding EDX line scans of GH3535 after corrosion for 100 h in molten (Li,Na,K)F + 0.09 M CrF_3 (a and b) and (Li,Na,K)F + 0.18 M CrF_3 (c and d) at 700 °C under Ar.

extremely hard to be removed completely. At high temperatures, H_2O may react with fluorides to generate gaseous HF by the following reactions:

$$MF(l) + H_2O = MOH(l) + HF(g) \quad (3)$$

$$2MF(l) + H_2O = M_2O(l) + 2HF(g) \quad (4)$$

M = Li, Na, K.

The generated HF may be dissolved partially into the melt and react with metals to form soluble metal fluorides:

$$Me + xHF(l) = MeF_x + \frac{x}{2}H_2(g) \quad (5)$$

Me = Ni, Fe, Cr, etc.

A higher H_2O content may produce a higher HF content, and thus cause a higher dissolution rate of metals. The thermodynamic stability of some common alloy constituents ranked by the free formation energy of their fluorides increases in the following order: Al < Cr < Fe < Co < Ni < Mo < W [1]. Thereby, the corrosion of GH3535 occurs mainly through the preferential dissolution of Cr into the melt. During the corrosion, Cr diffuses outward to react with HF to form CrF_2 which is then dissolved in the melt. The generated CrF_2 diffuses outward, and can be further oxidized to CrF_3 somewhere by the following reaction:

$$CrF_2 + HF = CrF_3 + \frac{1}{2}H_2 \quad (6)$$

Thus, the dissolution products of Cr in the melt exist as CrF_2 and CrF_3, with the free formation energy of CrF_3 slightly more positive

Table 5
Fitting results of the impedance spectra for the corrosion of GH3535 in molten (Li,Na,K)F-0.09M CrF_3 at 700 °C under Ar.

Time (h)	R_s ($\Omega\,cm^2$)	Y_{dl} ($\Omega^{-1}\,cm^{-2}\,s^{-n}$)	n_{dl}	R_t ($\Omega\,cm^2$)
2	2.39	4.02×10^{-2}	0.58	85.25
10	2.41	3.81×10^{-2}	0.66	95.96
18	2.46	4.12×10^{-2}	0.70	95.83
25	2.49	4.74×10^{-2}	0.71	96.11
38	2.58	5.83×10^{-2}	0.74	85.19
45	2.64	5.87×10^{-2}	0.74	86.81
52	4.32	5.01×10^{-2}	0.70	108.0
62	5.24	3.72×10^{-2}	0.69	125.6
80	5.25	3.82×10^{-2}	0.68	180.2
100	4.99	4.04×10^{-2}	0.68	188.1

Table 6
Fitting results of the impedance spectra for the corrosion of GH3535 in molten (Li,Na,K)F-0.18M CrF_3 at 700 °C under Ar.

Time (h)	R_s ($\Omega\,cm^2$)	Y_{dl} ($\Omega^{-1}\,cm^{-2}\,s^{-n}$)	n_{dl}	R_t ($\Omega\,cm^2$)
22	2.34	0.27	0.63	24.93
35	2.35	0.39	0.66	19.46
46	2.36	0.43	0.65	16.92
54	2.35	0.48	0.63	18.33
62	2.37	0.54	0.63	16.41
70	2.38	0.56	0.64	14.13
78	2.38	0.60	0.65	13.28
86	2.39	0.64	0.65	12.59
94	2.39	0.66	0.66	12.03
100	2.39	0.70	0.65	12.58

than that of CrF_2. In MSR, Cr^{3+} may also result from the disproportionation reaction of Cr^{2+}. High-valence Cr^{3+} may also act as an oxidizer to accelerate the dissolution of Cr [17]. A countercurrent diffusion of Cr^{2+}/Cr^{3+} could be expected to exist from the alloy/melt interface to the melt/gas interface, and the corrosion reaction could involve these species. CrF_3 could oxidize Cr by the following reaction:

$$2CrF_3 + Cr = 3CrF_2 \quad (7)$$

The above results show clearly that the presence of substantial concentrations of Cr^{3+} in the melt accelerates greatly the dissolution of Cr from the alloy GH3535.

The preferential dissolution of Cr gives rise to the generation of a Cr-depleted zone along the substrate alloy. Meanwhile, the outward diffusion of Cr can leave some vacancies in the substrate which then can aggregate to form internal voids. Moreover, the dissolution of Cr could also change the internal composition and thus the microstructures of the alloy, resulting in the precipitation of some new internal carbides in local regions including grain boundaries. When 5%H_2O was introduced, the formation of internal Cr-rich oxides is probably related to the internal penetration of fluorine and oxygen. This internal penetration could also involve the fluorine-carbide reactions, leading to the formation of some new carbides in some places [18].

3. Conclusions

The Ni-based alloy GH3535 is in active dissolution state at the corrosion potential in molten (Li,Na,K)F at 700 °C. The free corrosion current density of the alloy under Ar-5%H_2O is about 374 $\mu A\,cm^{-2}$ more than three times the value of 108 $\mu A\,cm^{-2}$ under pure Ar. The presence of 5%H_2O in Ar promotes both the anodic and cathodic reactions, and thus the corrosion. The Nyquist plots for the corrosion of the alloy under both atmospheres are all composed of a single capacitive loop, with smaller impedance values observed under 5%H_2O-containing atmosphere. The increase in the content of the impurity H_2O makes the melt be more aggressive, producing more HF which corrodes metals to form metal fluorides. The corrosion of the alloy occurs mainly through the reaction of Cr with HF to form soluble chromium fluorides including CrF_2 and CrF_3, giving rise to the formation of a Cr-depleted layer and large amounts of internal voids. Cr reacts firstly with HF to form CrF_2 which then can be oxidized to CrF_3. Multivalent transition metal Cr ions Cr^{2+}/Cr^{3+} are involved in the corrosion reactions. CrF_3 can act as an oxidizer to accelerate the dissolution of Cr from the alloy. When 5%H_2O is present in the system, the internal penetration of fluorine and oxygen could occur, with the formation of some internal Cr-rich oxides.

4. Experimental

The material used in the present study is a hot rolled Ni-based superalloy GH3535, whose chemical composition is listed in Table 1. From the microstructure of GH3535 shown in Fig. 1, it is observed that some Mo-rich $M_{23}C_6$ type carbides (black) are stripedly distributed along the rolling direction. The alloy plates were cut into specimens with a size of 5 mm × 30 mm × 2 mm by an electric spark cutting machine, followed by grinding down to 1000 grit SiC paper, cleaning with distilled water and then drying. A Fe–Cr wire was spot welded to one end of the specimen for electrical connection. The sample was then sealed in an alumina tube with high-temperature cement, with a length of 15 mm exposed. The cement was dried at room temperature for 24 h and then further solidified at 150 °C for 12 h. The exposed surfaces of the specimen were polished again with 1000 grit SiC paper, rinsed and dried prior to test.

All experiments were conducted in a closed stainless steel chamber under the protection of flowing high-purity Ar, as reported in Ref. [15]. A ternary eutectic mixture of 46.5LiF-11.5NaF-42KF (mole percent) was used for the corrosion study. After drying LiF, NaF and KF, respectively, a mixture of (Li,Na,K)F of 178.6 g was weighed and then put into a graphite crucible. The salt mixture was further dried at 200 °C in the reaction chamber under vacuum, and then under the protection of Ar for 20 h before the furnace was heated to the experimental temperature of 700 °C. To examine the effect of high valence transition metal Cr ions Cr^{3+} on the corrosion of the alloy, CrF_3 was added to the eutectic mixture of (Li,Na,K)F, with a mole fraction of 0.09 and 0.18, respectively. CrF_3 was also dried before preparing the mixed (Li,Na,K)-CrF_3 of 178.6 g.

To investigate the effect of the impurity H_2O on the corrosion behavior of the alloy in molten (Li,Na,K)F, pure Ar was allowed to pass through a closed isothermal water box to produce wet Ar before flowing into the reaction chamber. The temperature of the water box was kept at 33 °C corresponding to 5% water vapor.

All electrochemical measurements including potentiodynamic polarization and electrochemical impedance were conducted with a Princeton Applied Research PARSTAT 2273 potentiostat/Galvanostat system. Potentiodynamic polarization was undertaken at a scan rate of 20 mV min^{-1}, using a conventional three-electrode system with a Ni/NiF_2 electrode or a Pt electrode as the reference electrode and a graphite plate as the counter electrode. Electrochemical impedance measurements were carried out at open circuit potential between 0.01 Hz and 100 kHz using a two-electrode system (two working electrodes). The amplitude of input sin wave voltage was 10 mV.

The corroded samples were examined by scanning electron microscope (SEM) coupled with an energy dispersive X-ray spectrometer (EDX).

Acknowledgement

This work is supported by National Natural Science Foundation of China, Grant No. 51271190.

References

[1] L.C. Olson, J.W. Ambrosek, K. Sridharan, M.H. Anderson, T.R. Allen, J. Fluor. Chem. 130 (2009) 67–73.
[2] J.H. Devan, ORNL-TM-2021, Oak Ridge National Laboratory, 1969.
[3] L.C. Olson, University of Wisconsin-Madison, 2009.
[4] F.Y. Ouyang, C.H. Chang, B.C. You, T.K. Yeh, J.J. Kai, J. Nucl. Mater. 437 (2013) 201–207.
[5] M. Kondo, T. Nagasaka, V. Tsisar, A. Sagara, T. Muroga, T. Watanabe, T. Oshima, Y. Yokoyama, H. Miyamoto, E. Nakamura, N. Fujii, Fusion Eng. Des. 85 (2010) 1430–1436.
[6] D. Williams, L. Toth, K. Clarno, ORNL/TM-2006/12, Oak Ridge National Laboratory, 2006.
[7] M.W. Rosenthal, P.N. Haubenreich, R.B. Briggs, ORNL-4812, Oak Ridge National Laboratory, 1972.
[8] L. Olson, K. Sridharan, M. Anderson, T. Allen, Mater. High Temp. 27 (2010) 145–149.
[9] J.Y. Zheng, X.H. Yu, M. Liu, J.C. Zhang, J. Wang, Nucl. Technol. 34 (2011) 336–340.
[10] B. El-Dasher, J. Farmer, J. Ferreira, M.S. de Caro, A. Rubenchik, A. Kimura, J. Nucl. Mater. 419 (2011) 15–23.
[11] S. Fabre, C. Cabet, L. Cassayre, P. Chamelot, J. Finne, D. Noel, P. Taxil, Mater. Sci. Forum 595–598 (2008) 483–490.
[12] D. Ludwig, L. Olson, K. Sridharan, M. Anderson, T. Allen, Corros. Eng. Sci. Technol. 46 (2011) 360–364.
[13] M.W. Rosenthal, P.N. Haubenreich, R.B. Briggs, ORNL-4812, Oak Ridge National Laboratory, Oak Ridge, TN, USA, 1972.
[14] Y.X. Xu, Y.L. Wang, C.L. Zeng, High Temp. Mater. Process. (Lond.) 3 (2014) 269–276.
[15] Y.L. Wang, H.J. Liu, C.L. Zeng, J. Fluor. Chem. 165 (2014) 1–6.
[16] V.V. Ignat'ev, A.I. Surenkov, I.P. Gnidoi, V.I. Fedulov, V.S. Uglov, A.V. Panov, V.S. Sagaradze, V.G. Subbotin, A.D. Toropov, V.K. Afonichkin, A.L. Bove, At. Energy 101 (2006) 730–738.
[17] M. Sohal, M. Ebner, P. Sabharwall, P. Sharpe, INL/EXT-10-18297, 2010, p. 30.
[18] P. Elliott, A.A. Ansari, R. Prescott, M.F. Rothman, Corrosion/85, paper No. 13, National Association of Corrosion Engineers, Houston.